THE JOURNAL OF BIOLOGICAL CHEMISTRY VOL. 287, NO. 8, pp. 5253–5266, February 17, 2012

Small Molecule Structure Correctors Abolish Detrimental Effects of Apolipoprotein E4 in Cultured Neurons*[S]

Received for publication, June 28, 2011, and in revised form, November 28, 2011 Published, JBC Papers in Press, December 12, 2011, DOI 10.1074/jbc.M111.276162

Hung-Kai Chen[‡], Zhaoping Liu[‡], Anke Meyer-Franke[‡], Jens Brodbeck[‡], Rene D. Miranda[‡], James G. McGuire[‡], Michael A. Pleiss[‡], Zhong-Sheng Ji[‡], Maureen E. Balestra[‡], David W. Walker[‡], Qin Xu[‡§], Dah-eun Jeong[‡], Madhu S. Budamagunta[¶], John C. Voss[¶], Stephen B. Freedman[‡], Karl H. Weisgraber[‡§‖], Yadong Huang[‡§‖‡‡], and Robert W. Mahley[‡§‖**§§1]**

*From the [‡]Gladstone Center for Translational Research and [§]Gladstone Institute of Neurological Disease, San Francisco, California 94158, the Departments of [‖]Pathology, [§§]Medicine, and [‡‡]Neurology and the **Cardiovascular Research Institute, University of California, San Francisco, California 94143, and the [¶]Department of Biological Chemistry, School of Medicine, University of California, Davis, California 95616*

Background: Apolipoprotein E4 (apoE4), the major gene involved in Alzheimer disease, has a unique structure, intramolecular domain interaction, that is associated with neuropathology.
Results: Potent small molecule structure correctors block apoE4 domain interaction and reverse apoE4 detrimental effects in cultured neurons.
Conclusion: Structure correctors negate the detrimental effects of apoE4 in neurons.
Significance: ApoE4 structure correctors could represent a therapeutic approach for treating apoE4-associated neuropathology.

Apolipoprotein E4 (apoE4), the major genetic risk factor for late onset Alzheimer disease, assumes a pathological conformation, intramolecular domain interaction. ApoE4 domain interaction mediates the detrimental effects of apoE4, including decreased mitochondrial cytochrome *c* oxidase subunit 1 levels, reduced mitochondrial motility, and reduced neurite outgrowth *in vitro*. Mutant apoE4 (apoE4-R61T) lacks domain interaction, behaves like apoE3, and does not cause detrimental effects. To identify small molecules that inhibit domain interaction (*i.e.* structure correctors) and reverse the apoE4 detrimental effects, we established a high throughput cell-based FRET primary assay that determines apoE4 domain interaction and secondary cell- and function-based assays. Screening a ChemBridge library with the FRET assay identified CB9032258 (a phthalazinone derivative), which inhibits domain interaction in neuronal cells. In secondary functional assays, CB9032258 restored mitochondrial cytochrome *c* oxidase subunit 1 levels and rescued impairments of mitochondrial motility and neurite outgrowth in apoE4-expressing neuronal cells. These benefits were apoE4-specific and dose-dependent. Modifying CB9032258 yielded well defined structure-activity relationships and more active compounds with enhanced potencies in the FRET assay (IC_{50} of 23 and 116 nM, respectively). These compounds efficiently restored functional activities of apoE4-expressing cells in secondary assays. An EPR binding assay showed that the apoE4 structure correction resulted from direct interaction of a phthalazinone. With these data, a six-feature pharmacophore model was constructed for future drug design. Our results serve as a proof of concept that pharmacological intervention with apoE4 structure correctors negates apoE4 detrimental effects in neuronal cells and could be further developed as an Alzheimer disease therapeutic.

Apolipoprotein E4 (apoE4)[2] is the major genetic risk factor for late onset Alzheimer disease (AD), increasing the risk of developing AD at earlier ages of onset (1–3). In fact, 65–80% of all AD patients are carriers of at least one apoE4 allele (4). ApoE functions as a major carrier of lipids and cholesterol in both the peripheral and central nervous systems (5, 6). Human apoE has 299 amino acids with three common isoforms (apoE2, apoE3, and apoE4) that differ at residue 112 or 158. ApoE3 contains a cysteine at residue 112 and an arginine at residue 158, whereas apoE4 has arginine at both positions, and apoE2 has cysteine (5, 6). These minor variations give rise to profound differences in the tertiary protein structure and function (6–11). ApoE4 displays an intramolecular domain interaction between its amino- and carboxyl-terminal domains, leading to a compact structure (12, 13). Domain interaction in apoE4 is induced by Arg-112, which facilitates the formation of a salt bridge between Arg-61 in the amino-terminal domain and Glu-255 in the carboxyl-terminal domain (12, 13). The Cys-112 residue in apoE2 and apoE3 weakens the domain interaction, resulting in more open structures (13).

ApoE4 domain interaction was demonstrated by FRET in living neuronal cells (14). FRET is a well established technique

* This work was supported, in whole or in part, by National Institutes of Health Program Project Grant P01 AG022074. This work was also supported by Merck Research Laboratories.
[S] This article contains supplemental Fig. S1.
[1] To whom correspondence should be addressed: Gladstone Institute of Neurological Disease, 1650 Owens St., San Francisco, CA 94158. Tel.: 415-734-2061; Fax: 415-863-2250; E-mail: rmahley@gladstone.ucsf.edu.

[2] The abbreviations used are: apo, apolipoprotein; AD, Alzheimer disease; ANOVA, analysis of variance; DPBS, Dulbecco's PBS; eDHFR, *E. coli* dihydrofolate reductase; EC_{50}, half-maximal effective concentration; PLL, poly-L-lysine; MEM, minimum essential medium; mtCOX1, mitochondrial cytochrome *c* oxidase subunit 1; N2a, Neuro-2a; TMP-HEX, trimethoprim-hexachlorofluorescein conjugate; VDAC1, voltage-dependent anion channel isoform 1; NSE, neuron-specific enolase.

to detect changes in protein conformation or protein-protein interactions that relies on a distance-dependent transfer of photon energy between a donor and an acceptor fluorophore (15). The apoE4-FRET reporter showed a much stronger signal than the apoE3-FRET reporter, indicating that apoE4 has stronger domain interaction (14). The apoE-FRET specifically measures the interaction between the amino- and the carboxyl-terminal domains of apoE. Importantly, when threonine is substituted for arginine at residue 61 (R61T), this disrupts domain interaction in apoE4 and converts apoE4 to an "apoE3-like" molecule and decreases the FRET signal of apoE4 to the level of apoE3 in neuronal cells (14).

Evidence has suggested that domain interaction mediates a broad spectrum of apoE4 isoform-specific effects (8–11). In plasma, apoE4 binds preferentially to very low density lipoproteins (12, 13). Mutant apoE4-R61T lacking domain interaction, like apoE3, binds preferentially to high density lipoproteins (12, 13). In neurons, apoE4 reduces expression of the protein subunits of mitochondrial respiratory complexes, such as subunit 1 of complex IV (mtCOX1) and subunit α of complex V, resulting in a reduction in mitochondrial respiratory function (16). Unlike apoE4, apoE3 and apoE4-R61T did not induce mitochondrial dysfunction (16), suggesting that domain interaction mediates apoE4-specific detrimental effects on mitochondria. Similarly, apoE4 perturbs neuronal function by reducing mitochondrial motility, decreasing neurite outgrowth (17–19), and inhibiting synaptogenesis (20). In addition, amyloid β production in rat neuroblastoma cells is enhanced by apoE4 to a greater extent than apoE3 (21), whereas apoE4-R61T has no such effect (21). Unlike human apoE4, mouse apoE has threonine at residue 61, which prevents domain interaction (7). Introducing an apoE4-like domain interaction in mouse apoE by substituting arginine for threonine at the residue corresponding to amino acid 61 induces neurodegenerative pathology and memory deficits in the mice (22, 23). These detrimental effects of apoE4, which are mediated by domain interaction, probably contribute to AD pathogenesis (8–11). How apoE4 may be causative in AD has been reviewed previously (8).

Disrupting apoE4 domain interaction with small molecules, so-called apoE4 structure correctors, converts apoE4 into an apoE3-like conformation and reverses the apoE4-specific detrimental effects. We previously identified a prototype structure corrector, GIND-25, from an *in silico* screen (21). Treatment of neuronal cells with GIND-25 reduced the apoE4-enhanced amyloid β production (21) and restored mtCOX1 levels in apoE4-expressing cells (16). In addition, GIND-25 and a small molecule, PH-002, restored endoplasmic reticulum and Golgi apparatus transit of apoE4 in cultured neurons to levels equivalent to apoE3 and apoE4-R61T and rescued apoE4-caused impairment of neurite outgrowth and synaptogenesis (24). In the present study, we identified additional potent small molecules that inhibit domain interaction and thus reverse the detrimental effects of apoE4, using a high throughput, cell-based FRET primary screening assay that quantifies the change in apoE4 domain interaction and a panel of secondary cell- and function-based assays in neuronal cells. Screening a small molecule library led to the identification of phthalazinone analogs as a new class of apoE4 structure correctors that abolish apoE4 domain interaction-related detrimental effects in neuronal cells in culture.

EXPERIMENTAL PROCEDURES

Materials—Minimum essential medium (MEM) with Glutamax, Opti-MEM I, Dulbecco's PBS (DPBS) with or without calcium and magnesium, nonessential amino acids, sodium pyruvate, and G-418 were purchased from Invitrogen. FBS was purchased from HyClone, poly-L-lysine (PLL; 0.01% solution) from Sigma-Aldrich, and paraformaldehyde (16%) from Electron Microscopy Sciences. All chemicals were of analytical grade and were obtained from Sigma unless stated otherwise. (1-Oxyl-2,2,5,5-tetramethylpyrrolidin-3-yl)methyl methanethiosulfonate was from Toronto Research Chemicals (catalogue no. O873900); QuikChange multisite XL mutagenesis kit was from Stratagene. The phthalazinone CB9032258 (ChemBridge, San Diego, CA) and selected analogs from the Merck chemical compound library (Merck Research Laboratories, Boston, MA) were analyzed (Fig. 1).

Cell Culture and Cell Transfection—Neuro-2a cells stably expressing apoE3, apoE4, apoE4-R61T, or a control vector were described (25). Cells were routinely cultured in complete MEM with Glutamax containing 10% FBS, supplemented with nonessential amino acids, sodium pyruvate, and 400 μg/ml G-418 at 37 °C in a humidified 5% CO_2 incubator.

Generation of DNA Plasmids of sp-GFP-apoE4-eDHFR and sp-GFP-apoE3-eDHFR—A DNA fragment containing a human apoE signal peptide (sp) fused with GFP and apoE4 was PCR-amplified from a pcDNA-sp-GFP-apoE4 plasmid as described (24) using a primer pair of 5′-cacaagcttaccatgaaggttctgtgggctg-3′ and 5′-cacgaattccagtgattgtcgctgggcac-3′. The PCR fragment was then inserted into an *Escherichia coli* dihydrofolate reductase (eDHFR)-containing vector, pLL1 (Active Motif, Carlsbad, CA), to generate the expression construct sp-GFP-apoE4-eDHFR. The sp-GFP-apoE3-eDHFR construct was created from an sp-GFP-apoE4-eDHFR plasmid by mutagenesis using a QuikChange kit (Stratagene) and oligomers of 5′-catggaggacgtgtgcggccgcc-3′ and 5′-ggcggccgcacacgtcctccatg-3′, following the manufacturer's protocol. Neuro-2a cells were transfected with sp-GFP-apoE4-eDHFR, sp-GFP-apoE3-eDHFR, or a mixture of sp-GFP-apoE4 and eDHFR pLL1 (for expression of GFP-apoE4 and eDHFR from separate constructs) to establish stable transfectants as described (24, 25).

FRET Assay—Neuro-2a cells stably expressing the GFP/eDHFR FRET reporters were seeded at a density of 300,000 cells/well in 96-well plates and grown in riboflavin-free MEM with 10% FBS. Riboflavin was omitted to reduce background fluorescence. Two h after seeding, cells were loaded with a trimethoprim-hexachlorofluorescein conjugate (TMP-HEX, (LigandLink^{TM} Label, Active Motif) at 2 μM in culture medium and incubated for an additional 4 h. TMP is a cell-permeable and high affinity eDHFR ligand. After washing with PBS+ (PBS supplemented with 10 mM glucose, 0.9 mM $CaCl_2$, and 0.49 mM $MgCl_2$) three times, cells were incubated with various concentrations of compounds in riboflavin-free MEM without serum for 16 h. After washing once with PBS+, 200 μl of PBS+ was added to each well. Signals for both GFP (excitation, 485 nm; emission, 525 nm; cut-off, 515 nm) and FRET (excitation, 485

nm; emission, 565 nm; cut-off, 550 nm) were recorded on a Flexstation III (Molecular Devices, Sunnyvale, CA). The Z' is >0.5, S/B is 1.6 with a CV <10% and is tolerant of 1% DMSO or less.

Clones of Neuro-2a cells stably expressing GFP-apoE4-eDHFR at different levels were used to demonstrate that the expression level did not affect the FRET ratio. Five Neuro-2a clones (supplemental Fig. S1*A*) with increasing levels of GFP-apoE4-eDHFR were labeled with HEX, the GFP fluorescence and the FRET signal were measured, and the FRET ratio was calculated (supplemental Fig. S1*B*).

MtCOX1 In-cell Western Assay—Neuro-2a cells stably expressing apoE were seeded in 96-well black wall/clear bottom plates (Costar) at a density of 40,000 cells/well and incubated overnight in complete culture medium. At 70% confluence the following day, cells were carefully washed with PBS and changed to fresh Opti-MEM supplemented with MEM-NEAA and sodium pyruvate. For EC_{50} determination, each compound was tested in triplicate at seven concentrations (a 3-fold dilution series of 10,000 to 13.7 nM) plus mock control wells. The concentration of DMSO was kept at 0.5% in all of the wells. After a 24-h incubation, cells were fixed immediately with 4% paraformaldehyde in PBS for 20 min at room temperature and then washed three times with PBS containing 0.1% Triton X-100. An in-cell Western assay was performed using an in-cell Western kit (LI-COR Biosciences, Lincoln, NE), according to the manufacturer's protocol with minor modifications. Briefly, cells were incubated in blocking buffer for 1.5 h, followed by overnight incubation with 100 μl of blocking buffer without (for background control) or with mouse anti-mtCOX1 antibody (1:1000, MitoSciences, Eugene, OR; lots D0804 and E0594 displayed high specificity to purified COX1 and for COX1 in lysate from Neuro-2a cells expressing apoE3 and apoE4). Then the wells were washed three times in PBS containing 0.1% Tween 20 (Tween washing solution). Cells were then incubated in 50 μl of blocking buffer containing 0.2% Tween 20, IRDye 800CW-labeled anti-mouse secondary antibodies (1:800), Sapphire700 (1:1000, a nonspecific cell stain), and DRAQ5 (1:2000, a DNA dye). Fifty μl of the same staining solution were added to four empty wells (without cells) to determine background signals for Sapphire700/DRAQ5. We used Sapphire700 and DRAQ5 in combination for cell number normalization as suggested in the manufacturer's protocol. For background control (with cells), 50 μl of blocking buffer containing secondary antibodies alone (without Sapphire700 or DRAQ5) were added to the wells. After 1 h of incubation with the secondary antibodies, cells were washed three times with Tween washing solution and then once with PBS without Tween. After the final wash, the solution was removed completely from the wells. Signals from the 700- and 800-nm fluorophores were detected by scanning the plates on an Odyssey infrared imaging scanner immediately. Integrated intensity of the mtCOX1 immunoreactivity from each well was first normalized against the integrated intensity of Sapphire700/DRAQ5. Normalized mtCOX1 immunoreactivity from each compound-treated sample was then divided by the mean value from all mock control wells on the same plate (base line) to determine the percentage of changes in mtCOX1 immunoreactivity with drug. Activities of compounds were compared by their abilities to increase mtCOX1 immunoreactivity (percentage increase over the mock controls).

Mitochondrial Motility—PC12 pheochromocytoma cells stably expressing comparable levels of apoE (0.2 ng/mg protein) together with the mitochondrial marker mRFP were maintained in DMEM supplemented with 10% horse serum, 5% FCS, and 1 mM L-glutamine (all from Invitrogen). PC12 cells (7.5×10^3) were plated in 8-well chambered slides (Lab-Teq, Nunc) coated with PLL; differentiated in regular growth medium supplemented with 0.75% horse serum, 1 mM L-glutamine, and 40 ng/ml NGF; and used for experiments after 14 days of differentiation.

To determine if compounds that block apoE4 domain interaction rescue mitochondrial motility, differentiated PC12 cells were incubated with the indicated dose for 24 h. Digital images of mRFP fluorescence in neurites of PC12 cells differentiated with NGF for 14–16 days were captured at 10 frames/s for 10 s with a water-cooled EM-CCD camera (Hamamatsu, Bridgewater, NJ) mounted to an Axio Observer microscope (Zeiss) equipped with a ×60 oil objective. During recordings, cells were kept in CO_2-independent medium (Invitrogen) supplemented with 1 mM L-glutamine, 2.5% FCS, and 2.5% horse serum at 37 °C. Digital images were analyzed with NIH ImageJ software. The manual tracker plug-in was used to track and analyze mitochondrial movement. The percentage of motile mitochondria was (number of images in which the observed mitochondria are moving/number of recorded images) × 100.

To determine the effect on exogenous apoE, PC12 cells were cultured in DMEM supplemented with 5% horse serum, 2.5% FCS, and 1 mM L-glutamine. PC12 cells (25×10^4) were plated on 30-mm glass coverslips, coated with PLL, and differentiated in medium supplemented with 0.75% horse serum, 1 mM L-glutamine, and 40 ng/ml NGF. Differentiated PC12 cells were incubated for 24 h at 37 °C with 7.5 μg/ml of various forms of apoE, and mitochondrial dynamics were determined during a 15-min recording (12 frames/min) at room temperature. Recombinant human apoE, including the apoE4 variant carrying the R61T mutation, was prepared as described (12).

Neurite Outgrowth Assay—N2a-apoE3, N2a-apoE4, or N2a-apoE4-R61T cells grown to 80% confluence were seeded at a density of 8000 cells (N2a-apoE3) and 7500 cells (N2a-apoE4) per well into PLL-coated 24-well plates containing Opti-MEM with either 0.03% DMSO for control or various doses of compounds in quadruplicate. Cells were grown for 72 h at 37 °C to induce neurite outgrowth. After fixation with 4% paraformaldehyde for 30 min, cells were washed with DPBS and then stained by SimplyBlue™ Safe Stain (Invitrogen). Two h later, cells were washed with DPBS and kept in DPBS in the dark at 4 °C. Phase-contrast images were taken on an Axio Observer Z1 microscope equipped with a motorized stage using the Volocity software program. For each well, eight images were automatically taken from the same eight image fields. Images were analyzed using NIH ImageJ for total cell count per image and cells that had grown neurites longer than the cell body diameter.

Primary Neurons Treated with Structure Corrector—Primary neurons were obtained from the cortex and hippocampus of neuron-specific enolase (NSE)-apoE4 transgenic mice. The

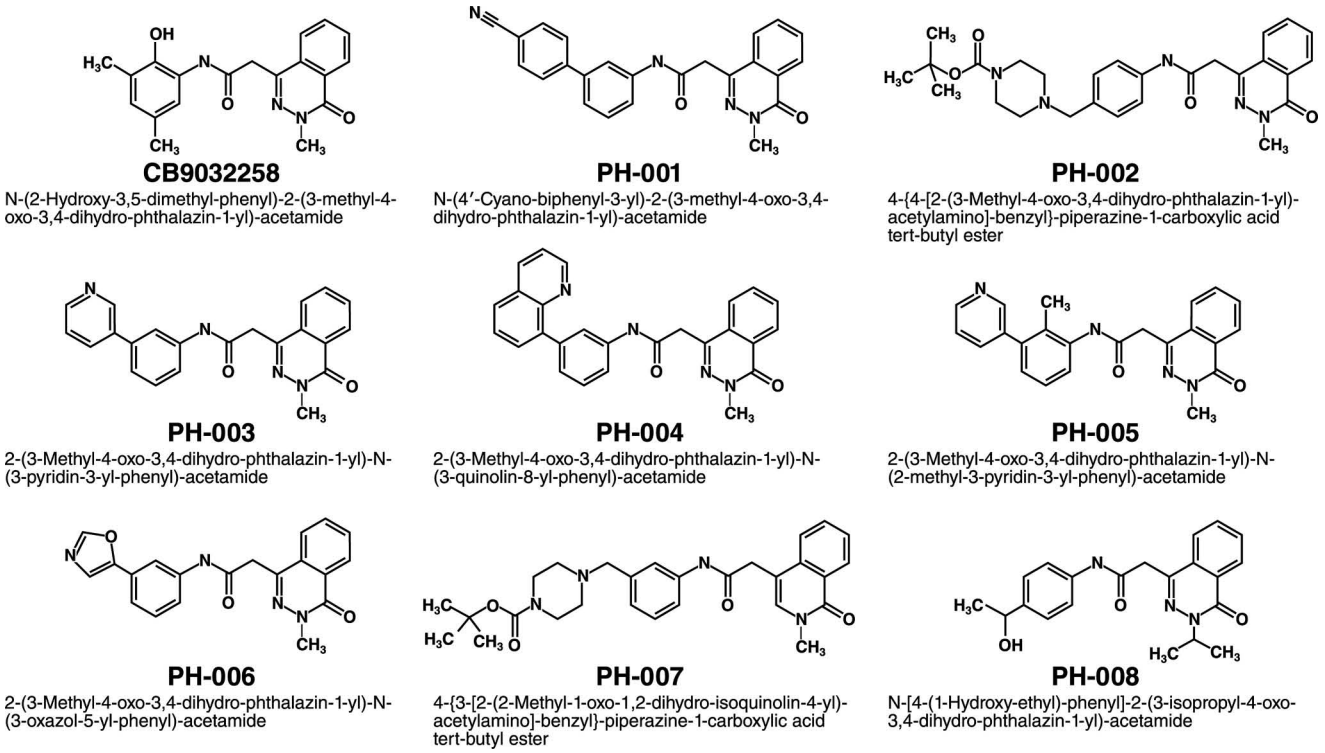

FIGURE 1. **Chemical structures of representative phthalazinone analogs.**

NSE mice have been fully characterized (26, 27). The cells were cultured for 10 days (28) and then treated with 200 nM PH-002 in DMSO for 4 days. Fresh compound was added on days 1 and 3, and then the cells were lysed on day 4 for Western blot analysis with anti-COX1 antibody. Voltage-dependent anion channel isoform 1 (VDAC1, mitochondrial porin) served as an internal control to monitor loading of sample on gels (Calbiochem, anti-mouse VDAC1).

ApoE4 Cys-76 Mutant Construct, Expression, and Purification—A cysteine mutation was introduced at position 76 into a cDNA encoding the apoE4 amino-terminal domain (residues 1–191) with a QuikChange mutagenesis kit and a modified pET32a construct as the template (9). The mutated sequence was verified by DNA sequencing. The apoE4 amino-terminal domain was expressed in *E. coli*. The cells were harvested and lysed, and cellular debris was pelleted as described (29). The apoE4 Cys-76 amino-terminal domain was purified as described (30) and spin-labeled as described for intact apoE4 cysteine mutants with (1-oxyl-2,2,5,5-tetramethylpyrrolidin-3-yl)methyl methanethiosulfonate (31).

EPR Experiments—EPR spectra were collected on a JEOL X-band spectrometer equipped with a loop-gap resonator. Spin-labeled apoE4 Cys-76 amino-terminal domain (25 μl, 57 μM) in TBS was incubated with an equal volume of PH-002 in TBS, prepared from a stock solution (500 μM in 10% DMSO/TBS) at two concentrations, 114 and 228 μM, respectively. After a 1-h incubation, ~4 μl of the mixture was placed in a sealed quartz capillary tube. Spectra from triplicate incubations were acquired at 20–22 °C with a single 60-s scan over 100 G at a microwave power of 2 milliwatts and a modulation amplitude optimized to the natural line width of the attached nitroxide. The effect of PH-002 was determined by comparing the effects on the central peak of the EPR spectra (h1/h0) of the compound and a control without compound.

Pharmacophore Modeling—Pharmacophore modeling was performed with the Pharmacophore Protocol within Discovery Studio version 2.1. Low energy conformations of all nine phthalazinone compounds in this report were determined with the CHARMm force field using the default potentials (Fig. 1). Multifeatured pharmacophores were constructed by generating common feature pharmacophores from the two most active compounds (PH-001 and PH-002). This procedure evaluates all possible hydrophobic, hydrogen bond acceptor, and donor features that the two compounds have in common, based on shared conformations. Up to 255 low energy conformations of each compound were included in the analysis. The algorithm starts with matching a small set of features and searches for more shared features until no further common conformation of the input compounds is found. Multiple hypotheses involving the spatial orientation of shared chemical features between the input compounds were generated and scored. All hypotheses were evaluated with the ligand pharmacophore mapping function and scoring module in the pharmacophore protocol and used to fit the remaining compounds.

Structure-based Pharmacophore Analysis—The high resolution crystal structure of the 22-kDa domain of human apoE4 (receptor binding domain, residues 1–165; Protein Data Bank entry 1GS9) was prepared for analysis using the Receptor-Ligand Interaction module within Discovery Studio version 2.1. Heteroatom molecules were removed from the structure, and a continuous dielectric was used in place of the water molecules. Missing hydrogens were added, valences were fixed where necessary, and atom types and

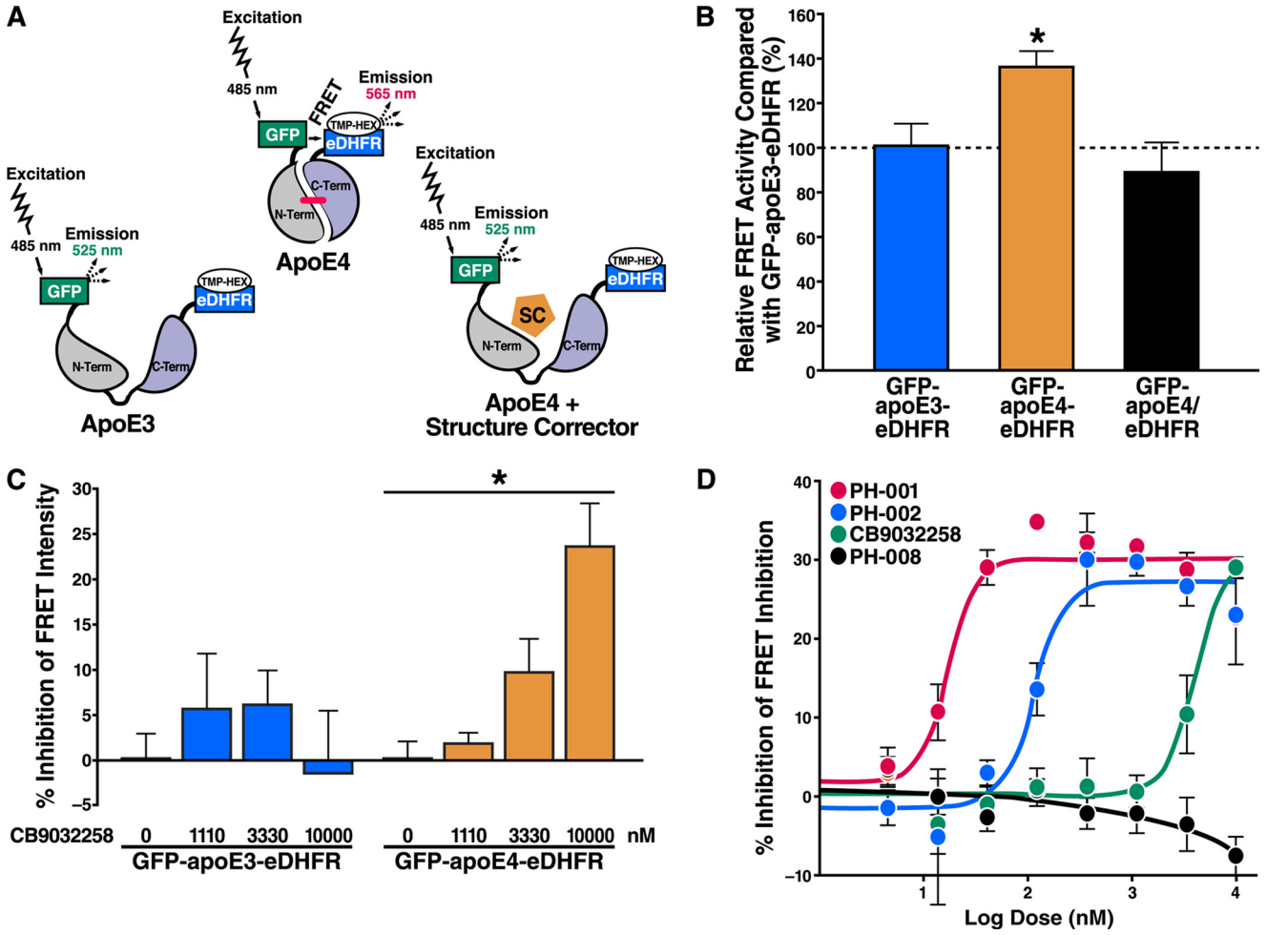

FIGURE 2. **FRET assay used to monitor intracellular apoE4 domain interaction in Neuro-2a cells and to identify apoE4 structure correctors.** *A*, apoE4 domain interaction allows FRET to occur between the donor and acceptor fluorophores. Inhibiting domain interaction by structure correctors reduces FRET from the apoE4 reporter. *SC*, structure corrector. *B*, FRET intensity (ratio of FRET signal divided by GFP signal) from GFP-apoE4-eDHFR is 36.3% higher than GFP-apoE3-eDHFR. *, $p < 0.0001$ ($n = 6$). FRET intensity from GFP-apoE4/eDHFR (expressing GFP-apoE4 and eDHFR by separate constructs, $n = 5$) is comparable with that of GFP-apoE3-eDHFR. *C*, CB9032258 inhibits FRET intensity from GFP-apoE4-eDHFR but not GFP-apoE3-eDHFR. *, $p < 0.05$, by ANOVA with Tukey's post hoc test. *D*, dose-response curves show relative potencies of PH-001, PH-002, CB9032258, and PH-008 to inhibit FRET intensity. Values are mean ± S.D. (*error bars*).

partial charges were assigned. The protein model was adjusted so that the optimal positions of polar hydrogens were identified. Steric clashes were removed by an energy minimization procedure. A binding site was built within 20 Å of Arg-61 in 1GS9, and an interaction map was generated in which all pharmacophore features (acceptors, donors, and hydrophobes) were created in the defined binding site. This resulted in ~1800 features. The features within 1GS9 served as a reference pharmacophore, and a pharmacophore comparison was conducted with the six-feature pharmacophore to find the closest match to the reference.

Statistical Analysis—Statistical analyses were performed by two-tailed *t* test or one-way analysis of variance (ANOVA) followed by Tukey's post hoc comparisons. $p < 0.05$ was considered statistically significant.

RESULTS

Establishing High Throughput Cell-based GFP-apoE-eDHFR FRET Assay for ApoE4 Structure Corrector Screening—Previously, we reported a CFP-apoE-YFP FRET system that was successfully used to demonstrate apoE4 domain interaction in living neuronal cells (14). To improve the assay performance in a high throughput format, we replaced the fluorophores by fusing a GFP (as a donor) to the amino terminus of apoE4 and an eDHFR to the carboxyl terminus of apoE4 (GFP-apoE4-eDHFR) (Fig. 2*A*). TMP-HEX served as the acceptor fluorophore. After loading with TMP-HEX, Neuro-2a cells expressing GFP-apoE4-eDHFR had a 36.3 ± 6.6% higher FRET signal (defined as the ratio of FRET to GFP) than those expressing GFP-apoE3-eDHFR ($p < 0.0001$, $n = 6$; Fig. 2*B*). The higher FRET signal of GFP-apoE4-eDHFR, compared with GFP-apoE3-eDHFR, reflects the closer proximity of the amino- and the carboxyl-terminal domains in apoE4. The GFP-apoE3-eDHFR signal was comparable with that in the cells expressing GFP-apoE4 and eDHFR from two separate constructs (GFP-apoE4/eDHFR, $n = 5$; Fig. 2*B*). Thus, the GFP-apoE-eDHFR FRET system sensitively detects conformational changes between the two intramolecular domains of apoE. Moreover, this assay allowed the development of a high throughput format (96 or

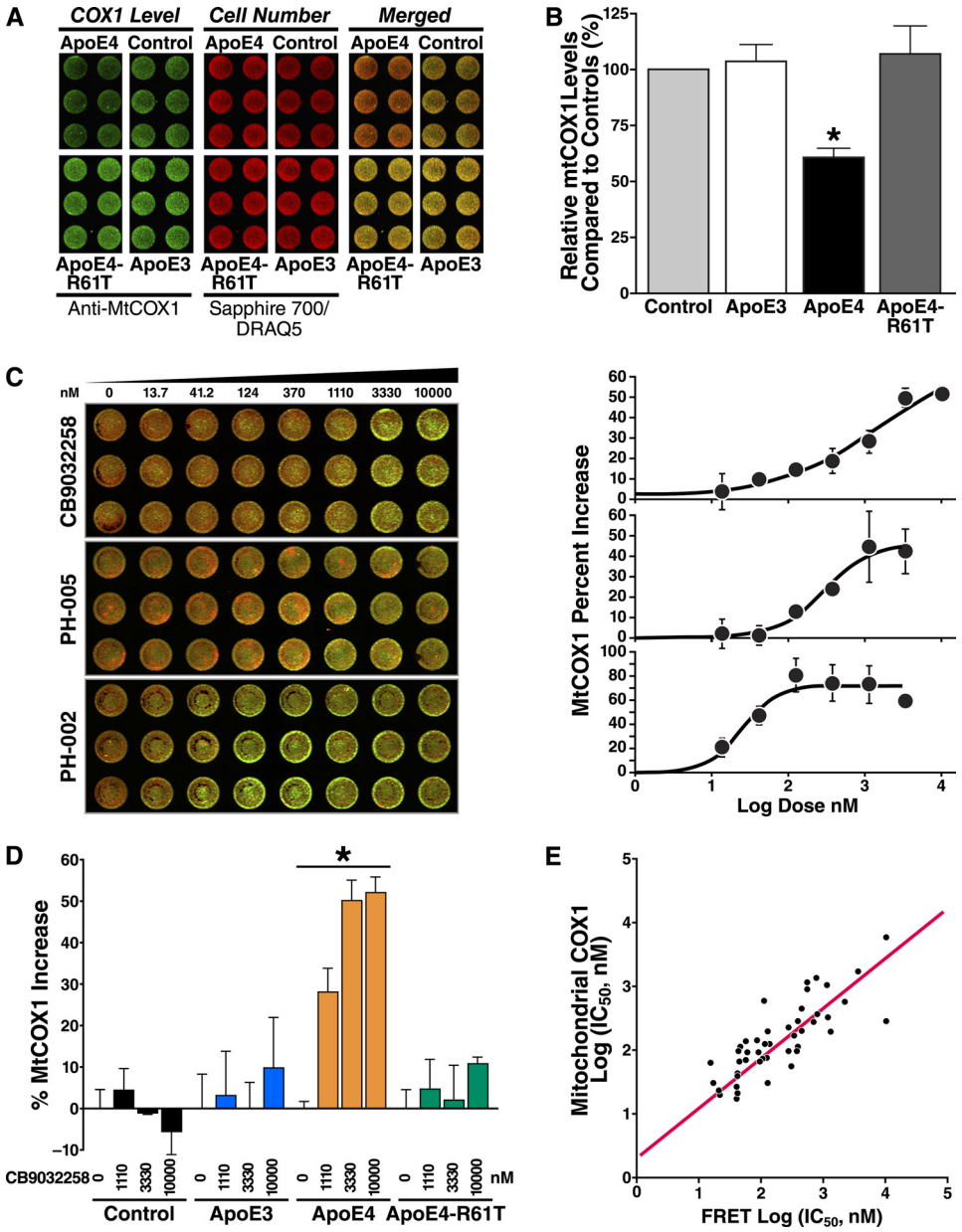

FIGURE 3. **MtCOX1 in-cell Western assay used to monitor apoE4-specific reduction of mtCOX1 in Neuro-2a cells and prevention of this impairment by apoE4 structure correctors.** *A*, representative images showing apoE4-specific reduction of mtCOX1 immunoreactivity. *Green*, anti-mtCOX1 immunofluorescence. *Red*, counterstain of Sapphire700 (a protein dye) and DRAQ5 (a DNA stain) for cell number normalization. A *merged image* of both channels is also shown. *B*, relative mtCOX1 levels in apoE4-expressing cells are significantly lower than in control cells or cells expressing apoE3 or apoE4-R61T. Values are mean ± S.D. (*error bars*) from three separate experiments. Signals from 15 wells were measured for every cell type in each experiment. *, $p < 0.001$ by ANOVA with Tukey's post hoc test. *C*, dose-dependent effects of CB9032258, PH-005, and PH-002 to restore mtCOX1 levels in apoE4-expressing cells. Shown on the *left* are *merged images* of mtCOX1 immunofluorescence (*green*) and Sapphire700/DRAQ5 counterstains (*red*) from cells treated with various doses of structure correctors. CB9032258 increases mtCOX1 levels only at doses of 3330 and 10,000 nM, whereas PH-005 is effective at lower doses (1110–10,000 nM). PH-002, the most active one, significantly increases mtCOX1 levels at a dose as low as 41.2 nM. The dose-response curves for the three compounds are shown on the *right*. Values are mean ± S.D. from triplicate wells. *D*, CB9032258 increases mtCOX1 levels only in apoE4-expressing cells and not in control cells or cells expressing apoE3 or apoE4-R61T. Values are mean ± S.D. from triplicate wells. *, $p < 0.01$ by ANOVA with Tukey's post hoc test. Similar results were obtained in at least three separate experiments. *E*, significant correlation of potencies between FRET and mtCOX1 assays. Pearson's $r = 0.803$, $R^2 = 0.645$, $p < 0.0001$, $n = 47$ phthalazinone analogs.

384 wells) for screening for small molecules that inhibit apoE4 domain interaction (Fig. 2*A*).

Establishing Cell- and Function-based Secondary Assays for ApoE4 Structure Corrector Validation—To identify small molecules that inhibit apoE4 domain interaction and also reverse the adverse effects caused by domain interaction, we established three cell- and function-based secondary assays for apoE4 structure corrector validation. First, we developed a 96-well format in-cell Western assay to monitor changes in mtCOX1 levels in neuronal cells. Mitochondria have emerged as a prime target for AD pathology (32) and the detrimental effects of apoE4 (16, 33–36). Steady-state levels of mtCOX1, an essential component of mitochondrial cytochrome *c* oxidase (complex IV), were significantly lower in Neuro-2a cells expressing apoE4 (N2a-apoE4) than in those expressing apoE3 (N2a-apoE3) or no apoE (control) (Fig. 3*A*, *left*). Unlike apoE4,

mutant apoE4-R61T had no such effect (Fig. 3*A*, *left*), suggesting that the reduction in mtCOX1 is a biological consequence of apoE4 domain interaction (16). The cell numbers in each well were comparable, as revealed by counterstaining for total protein (Sapphire700) and DNA (DRAQ5) (Fig. 3*A*, *middle*). ApoE4-specific reduction in mtCOX1 levels is readily detectable in the *merged image* of anti-mtCOX1 and Sapphire700/DRAQ5 (Fig. 3*A*, *right*) or by quantification of signal intensities from both channels on an Odyssey scanner (LI-COR) (Fig. 3*B*). After cell number normalization, the relative mtCOX1 levels in N2a-apoE4 cells were ~60 ± 4.8% ($n = 3$) of those in control cells, which were also significantly lower than those in N2a-apoE3 or N2a-apoE4-R61T cells (Fig. 3*B*, $p < 0.001$ by ANOVA). Therefore, the mtCOX1 in-cell Western assay can provide a biological readout for apoE4 domain interaction and thus for the validation of small molecules that inhibit domain interaction in neuronal cells.

Second, we developed a mitochondrial motility assay in differentiated PC12 cells. Mitochondrial motility was analyzed by time-lapse fluorescence microscopy (37). Differentiated PC12 cells incubated with exogenous apoE3 displayed 55–60% motile mitochondria, compared with only 25–30% motile mitochondria in apoE4-treated cells. ApoE4-R61T-treated cells gave results identical to those seen in apoE3-treated cells, demonstrating that domain interaction is mechanistically involved in apoE4-induced impairment of mitochondrial motility (Fig. 4*A*). Likewise, apoE4-expressing PC12 cells had a lower percentage of motile mitochondria (~30%), compared with apoE3-expressing cells (~60%) (Fig. 4*B*, control, no addition). This assay can be used to functionally validate apoE4 structure correctors.

Third, a neurite outgrowth assay of Neuro-2a cells was also developed by modifying our published protocol (17, 18). As reported, apoE4-expressing Neuro-2a cells had fewer cells with long neurites than those expressing apoE3 (Fig. 5*A*). Importantly, Neuro-2a cells expressing apoE4-R61T had neurite length similar to those expressing apoE3, which were significantly longer than those expressing apoE4. Again, these data indicate that apoE4 domain interaction is responsible for the apoE4-related neurite outgrowth impairment and thus can be used as an additional secondary assay to validate functionally the effect of apoE4 structure correctors.

Identification and Validation of CB9032258 as an ApoE4 Structure Corrector—A set of compounds from the ChemBridge library was selected for screening in our assays. CB9032258, a phthalazinone derivative, was found to reduce the FRET signal by 23.6 ± 1.7% ($n = 3$ at 10,000 nM) in GFP-apoE4-eDHFR but not in GFP-apoE3-eDHFR cells (Fig. 2*C*), suggesting that CB9032258 is a specific inhibitor of apoE4 domain interaction. The apoE4-specific inhibitory effect of CB9032258 on FRET is dose-dependent (IC_{50} = 4245 ± 2149 nM, $n = 3$) (Fig. 2*D* and Table 1).

CB9032258 was then functionally validated as a structure corrector in the cell-based secondary assays. Treatment of Neuro-2a cells expressing apoE4 with CB9032258 restored mtCOX1 levels to those seen in Neuro-2a cells expressing apoE3 (Fig. 3*C*). CB9032258-induced elevation of mtCOX1 immunoreactivity is dose-dependent, as shown by the percent-

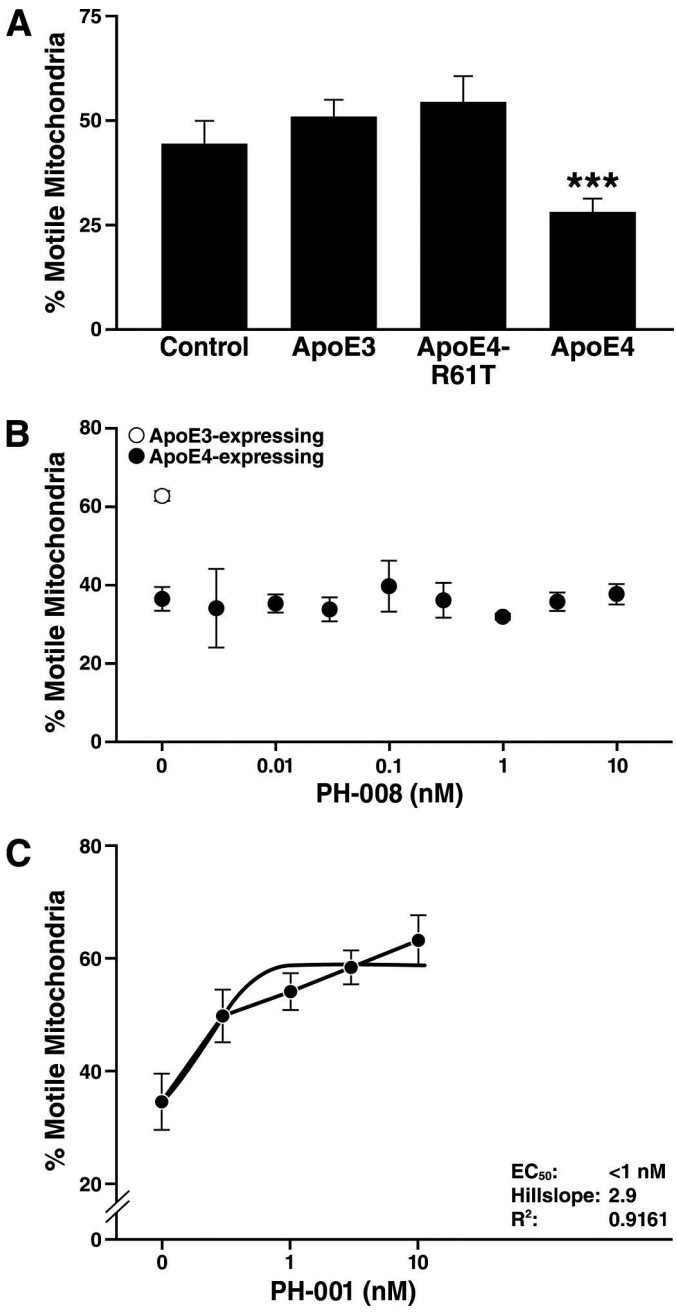

FIGURE 4. **Mitochondrial motility assay used to monitor apoE4-specific reduction in percentage of motile mitochondria and the reversibility of this impairment by apoE4 structure correctors.** *A*, differentiated PC12 cells were incubated for 24 h at 37 °C without (control) or with exogenous apoE3, apoE4, or apoE4-R61T (7.5 μg/ml). Mitochondrial dynamics, analyzed as a percentage of motile mitochondria, was measured during a 15-min recording (12 frames/min) (control, $n = 218$ mitochondria from 12 cells; apoE3, $n = 209$ mitochondria from 14 cells; apoE4, $n = 212$ mitochondria from nine cells; apoE4-R61T, $n = 164$ mitochondria from 12 cells). Values are mean ± S.E. (*error bars*). ***, $p < 0.001$ *versus* control (two-tailed *t* test). *B*, mitochondrial motility analyzed in apoE3- and apoE4-expressing PC12 cells at 37 °C without the addition of small molecules served as a control. After the addition of increasing doses of inactive PH-008 incubated for 24 h, the percentage of motile mitochondria was determined in the differentiated PC12 cells expressing apoE4 ($n = 100$ mitochondria from 10 cells in two separate experiments). Values are mean ± S.E. *C*, mitochondrial motility analyzed in apoE4-expressing PC12 cells at 37 °C with increasing concentrations of the active phthalazinone PH-001. Values are mean ± S.E. EC_{50}, Hill slope, and R^2 reported for the positive dose response.

age increase over the mock-treated cells (up to 52.3 ± 3.6% at 10,000 nM, EC_{50} = 2094 ± 544 nM, n = 3) (Fig. 3*C*, *top right*, and Table 1). CB9032258 treatment also abolished the apoE4 domain interaction-dependent detrimental effects on mitochondrial motility (EC_{50} = 30 nM) (Table 1) and neurite outgrowth (Fig. 5*B* and Table 1). Importantly, the beneficial effects of CB9032258 on mtCOX1 levels (Fig. 3*D*), mitochondrial motility, and neurite outgrowth (data not shown) were observed in apoE4-expressing cells but not in control (wild type) and/or apoE3-expressing cells. Thus, CB9032258 is functionally validated as an apoE4 structure corrector that can reverse the apoE4 domain interaction-dependent detrimental effects in neuronal cells in culture. It was chosen as a potential lead for further investigation.

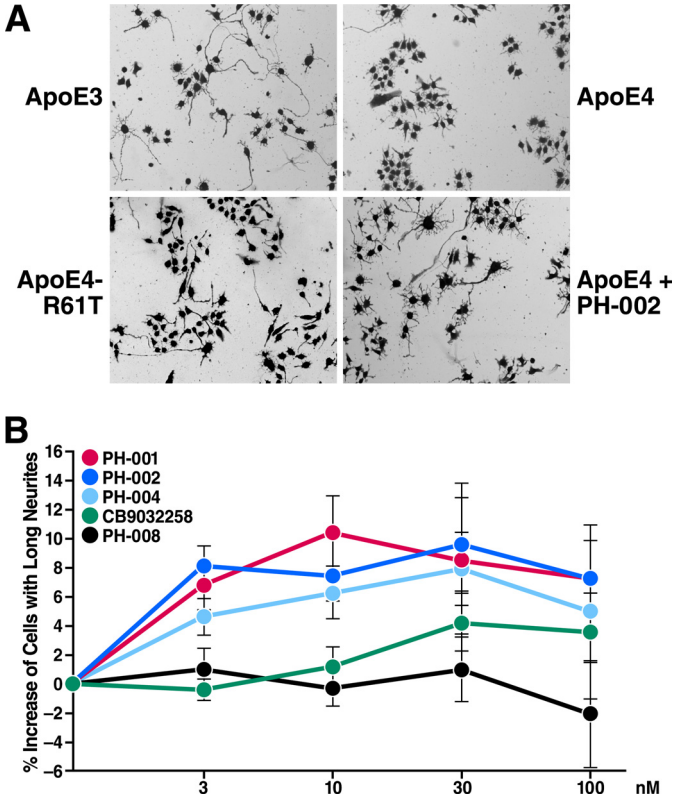

FIGURE 5. **Active phthalazinone analogs reverse apoE4-specific effects on neurite outgrowth.** *A*, representative images show that apoE4 expression is associated with fewer Neuro-2a cells with long neurites, whereas apoE3- and apoE4-R61T-expressing cells have similarly long neurites. ApoE4-expressing cells treated with the active phthalazinone PH-002 have similar long neurites resembling the apoE4-R61T cells. *B*, dose-response relationship of phthalazinone analogs on neurite outgrowth in apoE4-expressing Neuro-2a cells. Values are mean ± S.D. (*error bars*) (n = 4). p values (no addition controls *versus* neurite outgrowth with increasing concentration of structure correctors) were as follows: PH-001, PH-002, and PH-004 at 3 nM, $p < 0.0005$; PH-001 and PH-004 at 10 nM, $p < 0.0001$ (PH-002, $p = 0.003$); PH-001 and PH-002 at 30 nM, $p < 0.003$ (PH-004, $p < 0.0001$); PH-001, PH-002, PH-004, and CB9032258, $p = 0.0008$, $p = 0.007$, $p = 0.002$, and $p = 0.02$, respectively.

Analysis of Structure-Activity Relationships of Phthalazinone Analogs—To study the structure-activity relationships, 118 phthalazinone derivatives based on CB9032258 were obtained from Merck Research Laboratories (data not shown). Chemical modification of CB9032258 resulted in well defined structure-activity relationships, exemplified by the nine representative compounds shown in Fig. 1. Interestingly, the potencies of these compounds to inhibit domain interaction, as determined by the GFP-apoE4-eDHFR FRET assay, correlated well with their abilities to restore mtCOX1 levels in Neuro-2a cells expressing apoE4 (Table 1). For example, PH-001 (FRET IC_{50} = 23 nM) and PH-002 (FRET IC_{50} = 116 nM) were the most potent phthalazinones, with 185-fold and 37-fold enhanced FRET potencies over CB9032258, respectively (Fig. 2*D* and Table 1). They were also the most potent compounds in the secondary mtCOX1, mitochondrial motility, and neurite outgrowth assays (Figs. 3*C*, 4*C*, and 5*B* and Table 1). In fact, for the 47 phthalazinone analogs that were tested by both the FRET and the mtCOX1 assays, a strong positive correlation between FRET-IC_{50} and mtCOX1-EC_{50} was observed (Pearson's r = 0.8030, $p < 0.0001$) (Fig. 3*E*). In contrast, the inactive compounds identified in the FRET assay, PH-007 and PH-008, were also inactive in the mtCOX1 assay at the highest dose (10,000 nM) tested (Table 1), and PH-008 was also inactive in the mitochondrial motility (Fig. 4*B*) and neurite outgrowth (Fig. 5*B*) assays. The combination of the primary FRET assay and functional secondary assays identified potent phthalazinone analogs as a new class of apoE4 structure correctors.

PH-002 also was shown to increase COX1 levels in primary neurons from NSE-apoE4 transgenic mouse cortex and hippocampus. After 4 days of treatment with PH-002 (200 nM), COX1 levels were increased by ~60% (Fig. 6). We have previously demonstrated that PH-002 (100 nM) increased dendritic spine development in primary neurons from NSE-apoE4 trans-

TABLE 1

Phthalazinone compound potency in four different cell-based assays (mean ± S.D.)

Numbers in parentheses represent number of repeats.

Compound	FRET eDHFR assay[a]	COX1 mitochondrial protein level[b]	Mitochondrial motility[c]	Neurite outgrowth[d]
	nM	nM	nM	nM
PH-001	23 ± 10 (3)	19 ± 8 (5)	<1 (3)	1, 3 (2)
PH-002	116 ± 8 (3)	39 ± 22 (5)	<1 (3)	<3 (2)
PH-003	136 ± 12 (3)	116 ± 52 (3)		3 (2)
PH-004	238 ± 102 (3)	134 ± 74 (3)		1, 3 (2)
PH-005	706 ± 111 (3)	424 ± 260 (4)		
PH-006	870 ± 353 (3)	505 ± 100 (3)		
CB9032258	4245 ± 2149 (3)	2094 ± 540 (3)	30 (3)	30 (2)
PH-007	>10,000 (3)	>10,000 (3)		
PH-008	>10,000 (3)	>10,000 (4)	Inactive (2)	Inactive (2)

[a] IC_{50} for compounds that reduce the FRET signal in Neuro-2a cells stably expressing GFP-apoE4-eDHFR.
[b] EC_{50} for compounds that increase mtCOX1 immunofluorescence compared with the mock control.
[c] EC_{50} for compounds that increase mitochondrial motility in apoE4-expressing neurons.
[d] Expressed as minimal efficacious dose to significantly increase the number of N2a-apoE4 cells with long neurites.

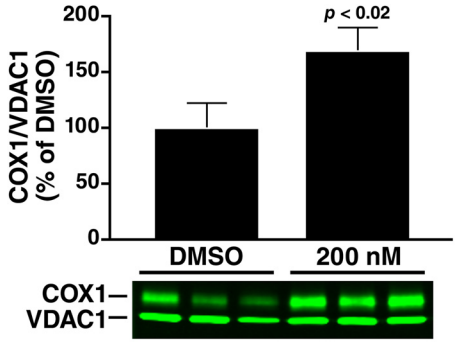

FIGURE 6. **PH-002 increases COX1 levels in primary neurons from NSE-apoE4 mouse cortex and hippocampus.** PH-002 (200 nM) was incubated with apoE4-expressing primary neurons for 4 days, and then the level of COX1 was determined by Western blot (mean ± S.D. (*error bars*) for three replicates). VDAC1 was used as the internal standard.

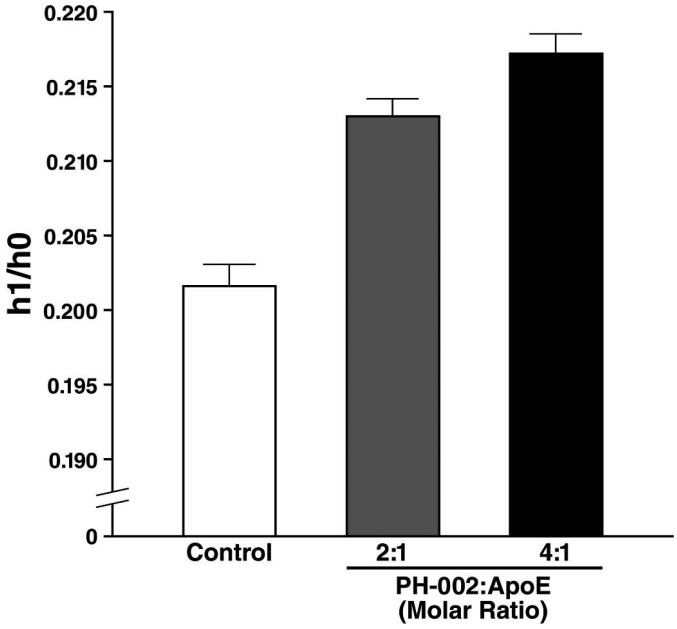

FIGURE 7. **Demonstration of direct binding of PH-002 to the apoE4 amino-terminal domain by EPR.** Incubation of the apoE4 amino-terminal domain with increasing concentrations of PH-002 resulted in a dose-dependent effect on the mobility of the spin label at position Cys-76, as determined from the effect on the control peak of the EPR spectra (h1/h0). Results are mean ± S.E. (*error bars*); control *versus* PH-002/apoE at ratios of 2:1 and 4:1; $p = 0.005$ and $p = 0.002$, respectively ($n = 3$).

genic mice to levels comparable with those in NSE-apoE3 primary neurons (apoE3-expressing primary neurons treated with PH-002 gave results identical to untreated primary neurons (24)).

EPR Demonstrating Direct Target Engagement—To demonstrate that PH-002 affected apoE4 structure through a direct binding mechanism, the apoE4 amino terminus spin-labeled at position 76 was incubated with PH-002 at two molar ratios, 2:1 and 4:1 (PH-002/apoE), and the effect on the motility of the Cys-76 spin label was determined. Position 76 was chosen because it is in the vicinity of the interface between the amino- and carboxyl-terminal domains of apoE4. A concentration-dependent effect of PH-002 on the mobility of the spin label was observed, demonstrating direct binding of PH-002 (Fig. 7).

Building Pharmacophore Model of Phthalazinones—The nine phthalazinone analogs (Fig. 1) display a good degree of structural diversity and well defined structure-activity relationships. These data allow us to build a pharmacophore model of phthalazinone for drug design. The best six-feature pharmacophore (Fig. 8*A*) is composed of three hydrophobic spheres (*blue*; the *spheres* are *labeled* "*A*", "*E*", and "*F*") and three hydrogen bond acceptors (*green arrows* with *arrowheads* pointing toward the donor (*labeled* "*B*", "*C*", and "*D*"). This model was based on the common features of the two most active compounds, PH-001 and PH-002.

Multiple hypotheses were derived from this analysis, and the model that best fit with all nine phthalazinones was selected. Fig. 8*B* shows the fit of PH-002 to the six-feature pharmacophore. This compound fits all six features, as expected. Fig. 8*C* shows a two-dimensional depiction of PH-002 annotated with the moieties making contact with these features. On the other hand, PH-008, an inactive compound, fits five of the six features, the exception being hydrophobe "F" (Fig. 8*D*), suggesting that hydrophobe "F" is necessary for activity. The other inactive compound, PH-007, only has five of the six features (Fig. 8*E*). This compound makes good contact with hydrophobe "F"; however, hydrogen bond acceptor "C" is not possible. The core ring structure is not a typical phthalazinone, but a 2-methyl-*2H*-isoquinolin-1-one that lacks acceptor functionality at this position. This result suggests that the hydrogen bond acceptor "*C*" is also required for activity.

Structure-based pharmacophore analysis is an independent way of confirming the results of the ligand-based methodology described above. Access to a high resolution crystal structure of the amino-terminal region of human apoE4 (12) allows the potential docking of the six-feature pharmacophore (Fig. 8*A*) into this binding domain. This type of analysis will confirm the importance of the two features ("C" and "F") identified in the above analysis. It is known that mutation of Arg-61 (R61T) (8–12) abolishes activity, so any docking model must include interaction with Arg-61. This was utilized as a starting point in this analysis. A binding site was built within 20 Å of Arg-61, and all possible pharmacophore features were identified within this binding site (all hydrophobes, acceptors, and donors). This resulted in ~1800 features. These features were used as a reference to find the best match for the six-feature pharmacophore described above. The results of this analysis are shown in Fig. 9*A*. PH-002 is docked into the 22-kDa amino-terminal region of human apoE4. This figure has the side chains of the 22-kDa domain removed except for Arg-61 (shown as *purple CPK spheres*), Arg-119 (shown as *yellow CPK spheres*), and Glu-50 (shown as *turquoise CPK spheres*). The structure of PH-002 is shown along with the six features described above (Fig. 8). Arg-61 shows a strong interaction with hydrophobe "F", which is consistent with the ligand-based findings described above. Glu-50 shows an interaction with hydrogen bond acceptor "C" that is consistent with the findings described. Arg-119 shows a tight interaction with hydrogen bond acceptor "B". Fig. 9*B* shows a close-up of PH-002 in the binding pocket. This structure-based analysis, in parallel with target engagement by EPR, confirms the results of the independent ligand-based approach.

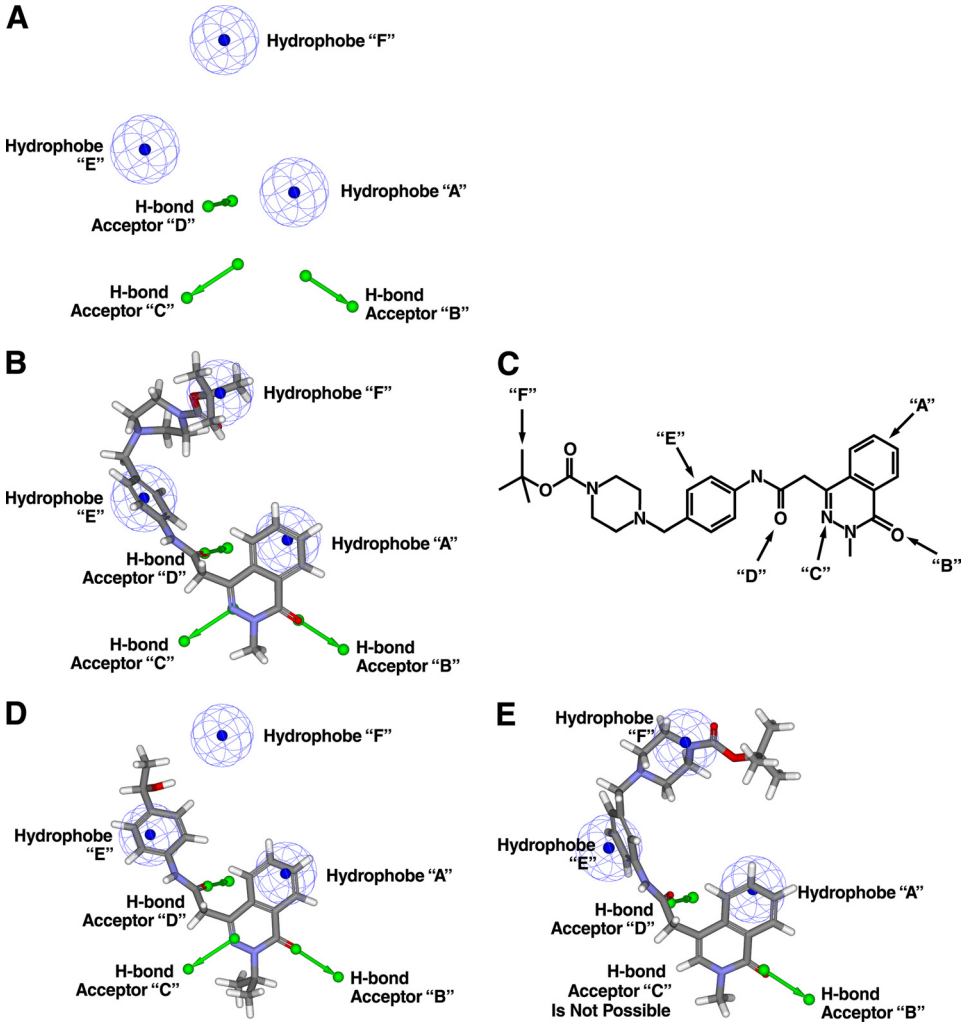

FIGURE 8. **Pharmacophore modeling for phthalazinone analogs using a ligand-based methodology.** *A*, phthalazinone pharmacophore. The six-feature pharmacophore is composed of three hydrophobic *spheres* (*blue*; *spheres* are *labeled* "*A*", "*E*", and "*F*") and three hydrogen bond acceptors (*green arrows* with *arrowheads* pointing toward donor *labeled* "*B*", "*C*", and "*D*"). *B*, pharmacophore fitted with PH-002. This potent compound fits all six features. *C*, two-dimensional structure of PH-002 annotated with moieties making contact with features of the pharmacophore. *D*, pharmacophore fitted with PH-008. This inactive compound fits five of the six features. Hydrophobe "F" is not satisfied, suggesting the importance of this feature for activity. *E*, pharmacophore fitted with PH-007. This inactive compound fits five of the six features. Hydrogen bond acceptor "C" is not possible with this compound. The core ring structure is not a phthalazinone but a 2-methyl-*2H*-isoquinolin-1-one, which lacks acceptor functionality at this position. Note that unlike PH-008, hydrophobe "F" is satisfied. The importance of the hydrogen bond acceptor "C" is suggested by the lack of activity of this compound.

DISCUSSION

The unique biophysical property characteristic of apoE4 (*i.e.* domain interaction between Arg-61 and Glu-255) markedly alters its structure and accounts for many of the functional features that distinguish apoE4 from apoE3 (6, 8, 9, 12, 13). The neuropathological features of apoE4 include (*a*) impaired neurite outgrowth (17–19); (*b*) disruption of the cytoskeleton in neurons (38), including increased Tau hyperphosphorylation (39, 40); (*c*) mitochondrial dysfunction in neurons, including altered mitochondrial membrane potential (36) and decreased respiratory enzyme levels and activity (16); (*d*) impaired neuronal mitochondrial motility (current study); (*e*) impaired synaptogenesis (20, 24); (*f*) enhanced susceptibility to neuron-specific proteolysis and neurotoxic fragment formation (39–41), (*g*) increased amyloid β production (21); (*h*) increased neuronal lysosomal leakage and apoptosis (42); (*i*) CNS neuropathology and impaired behavioral activity (26, 27, 41, 43), and (*j*) enhanced amyloid β deposition (44–47). All of these abnormal features (*a* through *i* above) that distinguish apoE4 from apoE3 are corrected or significantly improved by blocking apoE4 domain interaction by mutation of Arg-61 to threonine, small molecule structure correctors, or engineering of mouse apoE to alter domain interaction (8–11, 24).

This study was undertaken to identify a new potent (low nanomolar) class of structure corrector molecules that could be the basis for developing structure-activity relationships in a chemical series and to establish proof of concept that small molecules identified by their ability to alter the structure of apoE4 (*i.e.* block domain interaction) reduce its detrimental effects on neurons in culture. Previously, we identified several compounds of low potency (millimolar) that corrected apoE4 activity (21). However, these compounds lacked druglike properties.

The present study relied on small molecule library screening and chemical synthesis of lead compounds to identify struc-

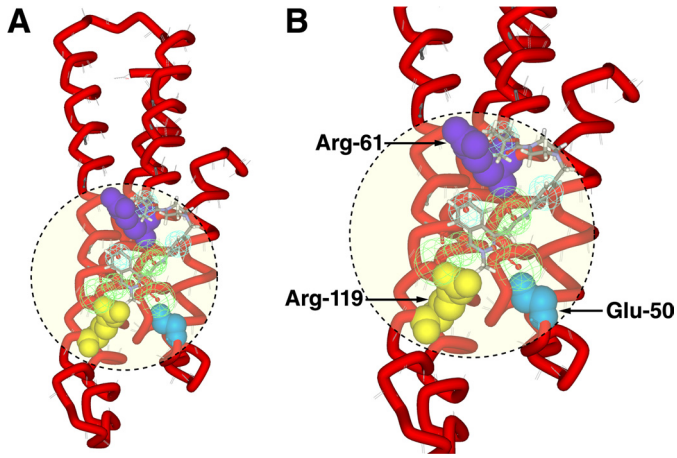

FIGURE 9. **Structure-based pharmacophore analysis docking the six-feature pharmacophore with the crystal structure of the amino-terminal domain of apoE4.** *A*, PH-002 docked into the 22-kDa domain of human apoE4 (Protein Data Bank entry 1GS9) utilizing the six-feature pharmacophore. *Purple CPK*, Arg-61, which is interacting with hydrophobe "F". *Yellow CPK*, Arg-119, which is interacting with the hydrogen bond acceptor "B". *B*, *close-up* of PH-002 docking.

ture-activity relationships. The phthalazinones represent such a series, demonstrating that the active compounds enter the cultured neurons and alter domain interaction, specifically in apoE4-expressing cells, without affecting apoE3-expressing cells. The active phthalazinones enhance neuronal mtCOX1 expression, restore mitochondrial motility, and promote neurite outgrowth to levels equivalent to apoE3. The critical importance of blocking domain interaction for restoring these functional activities was further established by showing that mutant apoE4-R61T, which lacks domain interaction, behaved like apoE3.

Previously, we demonstrated that the intracellular trafficking of apoE4 is impaired in the endoplasmic reticulum and Golgi apparatus of Neuro-2a cells expressing apoE4 compared with apoE3 trafficking, as determined by fluorescence recovery after photobleaching (24). ApoE4-R61T, which lacks domain interaction, gave results comparable with those for apoE3. Likewise, small molecule structure correctors GIND-25 (21) and PH-002 rescued the apoE4-impaired trafficking. In concert with the present data and the fluorescence recovery after photobleaching studies, two important points are made demonstrating where and how blocking domain interaction alters both the structure and function of apoE4. (*a*) small molecule structure correctors modulate domain interaction as soon as apoE4 is synthesized and/or enters the endoplasmic reticulum. Domain interaction has been shown to occur in poorly lipidated apoE4; however, when apoE complexes with lipids, the helical structure is significantly reorganized (9). (*b*) structure correctors, which rescue apoE4 intracellular trafficking, restore neurite outgrowth in apoE4-expressing Neuro-2a cells and dendritic spine development in primary hippocampal neurons from NSE-apoE4-expressing mice (no effects of structure correctors on apoE3-expressing Neuro-2a cells or apoE3-expressing primary neurons were observed).

The GFP-apoE4-eDHFR FRET system served as a relatively high throughput cell-based assay providing a signal that approximates the distance between the amino-terminal and carboxyl-terminal domains of apoE and identifying active small molecules that reduce the FRET signal intensity in apoE4. The FRET signal in the Neuro-2a cells expressing the GFP-apoE4-eDHFR was 36.3% higher than seen with GFP-apoE3-eDHFR (Fig. 2). After treatment of the cultured cells with potent small molecules (*i.e.* PH-001 and PH-002), the GFP-apoE4-eDHFR signal was inhibited by about 25–30% without significantly affecting the GFP-apoE3-eDHFR signal. Thus, this assay identifies apoE4-specific structure correctors.

The FRET data, which measure a biophysical structural property of apoE, correlate well with the mitochondrial COX1 in-cell Western data, which reflect a function property of apoE (Fig. 3*E*). Likewise, mitochondrial motility and neurite outgrowth represent downstream functional properties of apoE4 that are restored after treatment of the cells with the active small molecules. Furthermore, the inactive phthalazinones lacked potency across all assays, and the active phthalazinones modulated the activities only in the apoE4-expressing cells and not in apoE3-expressing cells.

In agreement with the apoE4-R61T mutant and the PH-002 studies indicating that disruption of apoE4 domain interaction reverses the effects of apoE4 in the FRET, mtCOX1, mitochondrial motility, and neurite outgrowth assays, PH-002 binds directly to the apoE4 amino-terminal domain. This provides direct evidence that PH-002 disrupts domain interaction by binding in the vicinity of the interface between the amino-terminal and carboxyl-terminal domains of apoE4. Structure-activity relationships established by the nine phthalazinone analogs allowed construction of a six-feature pharmacophore model. Important hydrophobic regions and hydrogen bond acceptors were identified in modeling the critical elements of the active phthalazinones. Docking of PH-002 onto the apoE4 22-kDa amino-terminal region suggested how the reactive molecules interact to form a binding pocket (Fig. 9). Thus, in agreement with EPR direct binding, pharmacophore modeling indicates how the phthalazinones interact with apoE4 and disrupt domain interaction, confirming the importance of Arg-61. These approaches can serve as a starting point for further optimization of apoE4 structure correctors.

Pharmacophore modeling has been proven to be successful for identifying various CNS drug targets (48–51), including catechol-*O*-methyl transferase (52), neuronal nicotinic acetylcholine receptor agonists (53), κ-opioid receptor agonists (54), $GABA_A$ (55), CNS ion channel modulators (56), and PDE4 (57). Results from the present study are also consistent. The six-feature pharmacophore model was built on the data in Table 1 and indicates that at least two of the features are essential for activity. This was confirmed by the structure-based modeling and is consistent with the EPR data establishing that residues in the vicinity of Arg-61 were essential for activity. The ligand-based approach can serve as a basis for further development of this important class of compounds.

The concept of structure correctors as a new therapeutic approach for certain targets and diseases has been gaining support since it arose about a decade ago (58–60). Protein structure and misfolding that affect intracellular transport and function occur commonly in human disease. The cystic fibrosis transmembrane conductance regulator cell surface chloride

channel is commonly mutated in cystic fibrosis (61). Approximately 80–90% of patients have a common deletion (F508 deletion) in the cystic fibrosis transmembrane conductance regulator protein that results in abnormal folding, retention in the endoplasmic reticulum, and impaired Cl^- secretory capacity. Several groups have discovered small molecules that bind and stabilize the protein, enhancing transit to the cell surface (structure correctors) and improving the ion channel function of receptors that reach the cell surface (potentiators) (62–65). The correctors increase cystic fibrosis transmembrane conductance regulator activity at low millimolar concentrations in cultured cells. Vertex Pharmaceuticals has completed a Phase IIa clinical trial on a structure corrector (VX-809) and a Phase III trial on a potentiator (VX-770) (see the United States Clinical Trials and Vertex Pharmaceuticals Web sites).

Fabry disease, a lipid storage disorder caused by mutations in α-galactosidase A, is also the target of structure corrector or pharmacological chaperone approaches to treatment. Mutated α-galactosidase A is retained in the endoplasmic reticulum and prematurely degraded before it reaches the lysosome; the normal α-galactosidase A lysosomal enzyme catabolizes the complex lipid globotriaoxylceramide (GL-3). The abnormal accumulation of this ceramide is responsible for an array of problems, including kidney failure, risk of myocardial infarction, and stroke (66–69). A small molecule has been identified (1-deoxygalactonojirimycin; migalastat) that binds and stabilizes the mutant enzyme, facilitating its transport to lysosomes (58, 70) and decreasing the accumulation of the ceramide by increasing the enzyme levels in cultured cells (71) and in transgenic mice (72). Phase II trials (Amicus Therapeutics; AT1001) showed long term safety and tolerability and a reduction in kidney GL-3 (73), and Phase III trials have commenced (74) (see the United States Clinical Trials Web site).

A structure corrector approach to restore normal function to p53 has also been actively investigated. Mutations in p53 result in an instability in the protein, preventing normal target interaction and usually causing accumulation to high concentrations in tumor cells. The mutant p53 prevents apoptosis and sustains tumor cell growth by impairing the ability of the p53 to bind to DNA and regulate gene transcription (75–77). Small molecules that restore p53 activity and conformation have been identified (77–82). One interesting compound, CP31398, a styrylquinazoline, restores the structure of mutant p53 to the normal conformation and rescues the p53 function in tumor cells (78, 82). Another class of compounds, called PRIMA-1 and APR-246, are pro-drugs that give rise to MQ, a reactive compound that binds to mutant p53 and enhances its apoptotic activity (83, 84). The active compound appears to modify thiol groups in the mutant, stabilizing the folding and restoring DNA binding (84). Clinical trials are beginning.

Thus, evidence is accumulating that small molecule structure correctors may be an effective approach to modulate biophysical properties and function of abnormal proteins. As shown in this paper, we identified structure correctors with high potency that modulate the structure of apoE4 by blocking or impairing intramolecular domain interaction. These same small molecules restore the functional intracellular activities of apoE4 to properties similar to those of apoE3 in cultured cells. Future studies will examine the *in vivo* effects of small molecule structure correctors and allow the design of active molecules that enter the CNS and block the detrimental effects of apoE4. Further structure-activity relationships will allow the identification of molecules that can be used to prevent or correct the detrimental effects of apoE4 in neuropathology.

Acknowledgments—We thank Sylvia Richmond for manuscript preparation, Stephen Ordway and Gary Howard for editorial assistance, and John C. W. Carroll for graphics. We are indebted to the staff of Merck Research Laboratories (Boston) for providing compounds from the Merck library and preparing specific phthalazinone analogs.

REFERENCES

1. Corder, E. H., Saunders, A. M., Strittmatter, W. J., Schmechel, D. E., Gaskell, P. C., Small, G. W., Roses, A. D., Haines, J. L., and Pericak-Vance, M. A. (1993) Gene dose of apolipoprotein E type 4 allele and the risk of Alzheimer's disease in late onset families. *Science* **261,** 921–923
2. Strittmatter, W. J., Saunders, A. M., Schmechel, D., Pericak-Vance, M., Enghild, J., Salvesen, G. S., and Roses, A. D. (1993) Apolipoprotein E. High-avidity binding to β-amyloid and increased frequency of type 4 allele in late-onset familial Alzheimer disease. *Proc. Natl. Acad. Sci. U.S.A.* **90,** 1977–1981
3. Saunders, A. M., Strittmatter, W. J., Schmechel, D., St George-Hyslop, P. H., Pericak-Vance, M. A., Joo, S. H., Rosi, B. L., Gusella, J. F., Crapper-MacLachlan, D. R., Alberts, M. J., Hulette, C., Crain, B., Goldgaber, D., and Roses, A. D. (1993) Association of apolipoprotein E allele ϵ4 with late-onset familial and sporadic Alzheimer's disease. *Neurology* **43,** 1467–1472
4. Farrer, L. A., Cupples, L. A., Haines, J. L., Hyman, B., Kukull, W. A., Mayeux, R., Myers, R. H., Pericak-Vance, M. A., Risch, N., and van Duijn, C. M. (1997) Effects of age, sex, and ethnicity on the association between apolipoprotein E genotype and Alzheimer disease. A meta-analysis. *JAMA* **278,** 1349–1356
5. Mahley, R. W. (1988) Apolipoprotein E. Cholesterol transport protein with expanding role in cell biology. *Science* **240,** 622–630
6. Mahley, R. W., Weisgraber, K. H., and Huang, Y. (2009) Apolipoprotein E. Structure determines function, from atherosclerosis to Alzheimer's disease to AIDS. *J. Lipid Res.* **50,** S183–S188
7. Weisgraber, K. H. (1994) Apolipoprotein E. Structure-function relationships. *Adv. Protein Chem.* **45,** 249–302
8. Mahley, R. W., Weisgraber, K. H., and Huang, Y. (2006) Apolipoprotein E4. A causative factor and therapeutic target in neuropathology, including Alzheimer's disease. *Proc. Natl. Acad. Sci. U.S.A.* **103,** 5644–5651
9. Zhong, N., and Weisgraber, K. H. (2009) Understanding the association of apolipoprotein E4 with Alzheimer disease. Clues from its structure. *J. Biol. Chem.* **284,** 6027–6031
10. Mahley, R. W., and Huang, Y. (2009) Alzheimer disease. Multiple causes, multiple effects of apolipoprotein E4, and multiple therapeutic approaches. *Ann. Neurol.* **65,** 623–625
11. Huang, Y. (2010) Aβ-independent roles of apolipoprotein E4 in the pathogenesis of Alzheimer's disease. *Trends Mol. Med.* **16,** 287–294
12. Dong, L. M., Wilson, C., Wardell, M. R., Simmons, T., Mahley, R. W., Weisgraber, K. H., and Agard, D. A. (1994) Human apolipoprotein E. Role of arginine 61 in mediating the lipoprotein preferences of the E3 and E4 isoforms. *J. Biol. Chem.* **269,** 22358–22365
13. Dong, L. M., and Weisgraber, K. H. (1996) Human apolipoprotein E4 domain interaction. Arginine 61 and glutamic acid 255 interact to direct the preference for very low density lipoproteins. *J. Biol. Chem.* **271,** 19053–19057
14. Xu, Q., Brecht, W. J., Weisgraber, K. H., Mahley, R. W., and Huang, Y. (2004) Apolipoprotein E4 domain interaction occurs in living neuronal cells as determined by fluorescence resonance energy transfer. *J. Biol. Chem.* **279,** 25511–25516
15. Zhang, J., Campbell, R. E., Ting, A. Y., and Tsien, R. Y. (2002) Creating new fluorescent probes for cell biology. *Nat. Rev. Mol. Cell Biol.* **3,** 906–918

16. Chen, H. K., Ji, Z. S., Dodson, S. E., Miranda, R. D., Rosenblum, C. I., Reynolds, I. J., Freedman, S. B., Weisgraber, K. H., Huang, Y., and Mahley, R. W. (2011) Apolipoprotein E4 domain interaction mediates detrimental effects on mitochondria and is a potential therapeutic target for Alzheimer disease. *J. Biol. Chem.* **286,** 5215–5221
17. Nathan, B. P., Bellosta, S., Sanan, D. A., Weisgraber, K. H., Mahley, R. W., and Pitas, R. E. (1994) Differential effects of apolipoproteins E3 and E4 on neuronal growth *in vitro*. *Science* **264,** 850–852
18. Bellosta, S., Nathan, B. P., Orth, M., Dong, L. M., Mahley, R. W., and Pitas, R. E. (1995) Stable expression and secretion of apolipoproteins E3 and E4 in mouse neuroblastoma cells produces differential effects on neurite outgrowth. *J. Biol. Chem.* **270,** 27063–27071
19. Holtzman, D. M., Pitas, R. E., Kilbridge, J., Nathan, B., Mahley, R. W., Bu, G., and Schwartz, A. L. (1995) Low density lipoprotein receptor-related protein mediates apolipoprotein E-dependent neurite outgrowth in a central nervous system-derived neuronal cell line. *Proc. Natl. Acad. Sci. U.S.A.* **92,** 9480–9484
20. Brodbeck, J., Balestra, M. E., Saunders, A. M., Roses, A. D., Mahley, R. W., and Huang, Y. (2008) Rosiglitazone increases dendritic spine density and rescues spine loss caused by apolipoprotein E4 in primary cortical neurons. *Proc. Natl. Acad. Sci. U.S.A.* **105,** 1343–1346
21. Ye, S., Huang, Y., Müllendorff, K., Dong, L., Giedt, G., Meng, E. C., Cohen, F. E., Kuntz, I. D., Weisgraber, K. H., and Mahley, R. W. (2005) Apolipoprotein (apo) E4 enhances amyloid β peptide production in cultured neuronal cells. ApoE structure as a potential therapeutic target. *Proc. Natl. Acad. Sci. U.S.A.* **102,** 18700–18705
22. Raffai, R. L., Dong, L. M., Farese, R. V., Jr., and Weisgraber, K. H. (2001) Introduction of human apolipoprotein E4 "domain interaction" into mouse apolipoprotein E. *Proc. Natl. Acad. Sci. U.S.A.* **98,** 11587–11591
23. Zhong, N., Scearce-Levie, K., Ramaswamy, G., and Weisgraber, K. H. (2008) Apolipoprotein E4 domain interaction. Synaptic and cognitive deficits in mice. *Alzheimers Dement.* **4,** 179–192
24. Brodbeck, J., McGuire, J., Liu, Z., Meyer-Franke, A., Balestra, M. E., Jeong, D. E., Pleiss, M., McComas, C., Hess, F., Witter, D., Peterson, S., Childers, M., Goulet, M., Liverton, N., Hargreaves, R., Freedman, S., Weisgraber, K. H., Mahley, R. W., and Huang, Y. (2011) Structure-dependent impairment of intracellular apolipoprotein E4 trafficking and its detrimental effects are rescued by small-molecule structure correctors. *J. Biol. Chem.* **286,** 17217–17226
25. Harris, F. M., Tesseur, I., Brecht, W. J., Xu, Q., Mullendorff, K., Chang, S., Wyss-Coray, T., Mahley, R. W., and Huang, Y. (2004) Astroglial regulation of apolipoprotein E expression in neuronal cells. Implications for Alzheimer's disease. *J. Biol. Chem.* **279,** 3862–3868
26. Buttini, M., Orth, M., Bellosta, S., Akeefe, H., Pitas, R. E., Wyss-Coray, T., Mucke, L., and Mahley, R. W. (1999) Expression of human apolipoprotein E3 or E4 in the brains of Apoe$^{-/-}$ mice. Isoform-specific effects on neurodegeneration. *J. Neurosci.* **19,** 4867–4880
27. Raber, J., Wong, D., Buttini, M., Orth, M., Bellosta, S., Pitas, R. E., Mahley, R. W., and Mucke, L. (1998) Isoform-specific effects of human apolipoprotein E on brain function revealed in ApoE knockout mice. Increased susceptibility of females. *Proc. Natl. Acad. Sci. U.S.A.* **95,** 10914–10919
28. Li, G., Bien-Ly, N., Andrews-Zwilling, Y., Xu, Q., Bernardo, A., Ring, K., Halabisky, B., Deng, C., Mahley, R. W., and Huang, Y. (2009) GABAergic interneuron dysfunction impairs hippocampal neurogenesis in adult apolipoprotein E4 knockin mice. *Cell Stem Cell* **5,** 634–645
29. Morrow, J. A., Arnold, K. S., and Weisgraber, K. H. (1999) Functional characterization of apolipoprotein E isoforms overexpressed in *Escherichia coli*. *Protein Expr. Purif.* **16,** 224–230
30. Hatters, D. M., Peters-Libeu, C. A., and Weisgraber, K. H. (2005) Engineering conformational destabilization into mouse apolipoprotein E. A model for a unique property of human apolipoprotein E4. *J. Biol. Chem.* **280,** 26477–26482
31. Hatters, D. M., Budamagunta, M. S., Voss, J. C., and Weisgraber, K. H. (2005) Modulation of apolipoprotein E structure by domain interaction. Differences in lipid-bound and lipid-free forms. *J. Biol. Chem.* **280,** 34288–34295
32. Mosconi, L., Pupi, A., and De Leon, M. J. (2008) Brain glucose hypometabolism and oxidative stress in preclinical Alzheimer's disease. *Ann. N.Y. Acad. Sci.* **1147,** 180–195
33. Small, G. W., Mazziotta, J. C., Collins, M. T., Baxter, L. R., Phelps, M. E., Mandelkern, M. A., Kaplan, A., La Rue, A., Adamson, C. F., Chang, L., Guze, B. H., Corder, E. H., Saunders, A. M., Haines, J. L., Pericak-Vance, M. A., and Roses, A. D. (1995) Apolipoprotein E type 4 allele and cerebral glucose metabolism in relatives at risk for familial Alzheimer disease. *JAMA* **273,** 942–947
34. Reiman, E. M., Chen, K., Alexander, G. E., Caselli, R. J., Bandy, D., Osborne, D., Saunders, A. M., and Hardy, J. (2004) Functional brain abnormalities in young adults at genetic risk for late-onset Alzheimer's dementia. *Proc. Natl. Acad. Sci. U.S.A.* **101,** 284–289
35. Reiman, E. M., Chen, K., Alexander, G. E., Caselli, R. J., Bandy, D., Osborne, D., Saunders, A. M., and Hardy, J. (2005) Correlations between apolipoprotein E ϵ4 gene dose and brain-imaging measurements of regional hypometabolism. *Proc. Natl. Acad. Sci. U.S.A.* **102,** 8299–8302
36. Chang, S., ran Ma, T., Miranda, R. D., Balestra, M. E., Mahley, R. W., and Huang, Y. (2005) Lipid- and receptor-binding regions of apolipoprotein E4 fragments act in concert to cause mitochondrial dysfunction and neurotoxicity. *Proc. Natl. Acad. Sci. U.S.A.* **102,** 18694–18699
37. Vossel, K. A., Zhang, K., Brodbeck, J., Daub, A. C., Sharma, P., Finkbeiner, S., Cui, B., and Mucke, L. (2010) Tau reduction prevents Aβ-induced defects in axonal transport. *Science* **330,** 198
38. Nathan, B. P., Chang, K. C., Bellosta, S., Brisch, E., Ge, N., Mahley, R. W., and Pitas, R. E. (1995) The inhibitory effect of apolipoprotein E4 on neurite outgrowth is associated with microtubule depolymerization. *J. Biol. Chem.* **270,** 19791–19799
39. Huang, Y., Liu, X. Q., Wyss-Coray, T., Brecht, W. J., Sanan, D. A., and Mahley, R. W. (2001) Apolipoprotein E fragments present in Alzheimer's disease brains induce neurofibrillary tangle-like intracellular inclusions in neurons. *Proc. Natl. Acad. Sci. U.S.A.* **98,** 8838–8843
40. Brecht, W. J., Harris, F. M., Chang, S., Tesseur, I., Yu, G. Q., Xu, Q., Dee Fish, J., Wyss-Coray, T., Buttini, M., Mucke, L., Mahley, R. W., and Huang, Y. (2004) Neuron-specific apolipoprotein E4 proteolysis is associated with increased tau phosphorylation in brains of transgenic mice. *J. Neurosci.* **24,** 2527–2534
41. Harris, F. M., Brecht, W. J., Xu, Q., Tesseur, I., Kekonius, L., Wyss-Coray, T., Fish, J. D., Masliah, E., Hopkins, P. C., Scearce-Levie, K., Weisgraber, K. H., Mucke, L., Mahley, R. W., and Huang, Y. (2003) Carboxyl-terminal-truncated apolipoprotein E4 causes Alzheimer's disease-like neurodegeneration and behavioral deficits in transgenic mice. *Proc. Natl. Acad. Sci. U.S.A.* **100,** 10966–10971
42. Ji, Z. S., Miranda, R. D., Newhouse, Y. M., Weisgraber, K. H., Huang, Y., and Mahley, R. W. (2002) Apolipoprotein E4 potentiates amyloid β peptide-induced lysosomal leakage and apoptosis in neuronal cells. *J. Biol. Chem.* **277,** 21821–21828
43. Raber, J., Wong, D., Yu, G. Q., Buttini, M., Mahley, R. W., Pitas, R. E., and Mucke, L. (2000) Apolipoprotein E and cognitive performance. *Nature* **404,** 352–354
44. Holtzman, D. M., Bales, K. R., Tenkova, T., Fagan, A. M., Parsadanian, M., Sartorius, L. J., Mackey, B., Olney, J., McKeel, D., Wozniak, D., and Paul, S. M. (2000) Apolipoprotein E isoform-dependent amyloid deposition and neuritic degeneration in a mouse model of Alzheimer's disease. *Proc. Natl. Acad. Sci. U.S.A.* **97,** 2892–2897
45. Bales, K. R., Verina, T., Cummins, D. J., Du, Y., Dodel, R. C., Saura, J., Fishman, C. E., DeLong, C. A., Piccardo, P., Petegnief, V., Ghetti, B., and Paul, S. M. (1999) Apolipoprotein E is essential for amyloid deposition in the APP^{V717F} transgenic mouse model of Alzheimer's disease. *Proc. Natl. Acad. Sci. U.S.A.* **96,** 15233–15238
46. Irizarry, M. C., Cheung, B. S., Rebeck, G. W., Paul, S. M., Bales, K. R., and Hyman, B. T. (2000) Apolipoprotein E affects the amount, form, and anatomical distribution of amyloid β-peptide deposition in homozygous APP^{V717F} transgenic mice. *Acta Neuropathol.* **100,** 451–458
47. Bien-Ly, N., Andrews-Zwilling, Y., Xu, Q., Bernardo, A., Wang, C., and Huang, Y. (2011) C-terminal-truncated apolipoprotein (apo) E4 inefficiently clears amyloid-β (Aβ) and acts in concert with Aβ to elicit neuronal and behavioral deficits in mice. *Proc. Natl. Acad. Sci. U.S.A.* **108,** 4236–4241
48. Güner, O., Clement, O., and Kurogi, Y. (2004) Pharmacophore modeling

and three-dimensional database searching for drug design using Catalyst. Recent advances. *Curr. Med. Chem.* **11,** 2991–3005
49. Martin, Y. C. (2007) in *Comprehensive Medicinal Chemistry II* (Mason, J. S., Taylor, J. B., and Triggle, D. J., eds) Vol. 4, pp. 119–147, Elsevier, Oxford
50. Martin, Y. C. (2007) in *Comprehensive Medicinal Chemistry II* (Mason, J. S., Taylor, J. B., and Triggle, D. J., eds) Vol. 4, pp. 515–536, Elsevier, Oxford
51. Wolber, G., Seidel, T., Bendix, F., and Langer, T. (2008) Molecule-pharmacophore superpositioning and pattern matching in computational drug design. *Drug Discov. Today* **13,** 23–29
52. Lee, J. Y., Baek, S., and Kim, Y. (2007) Receptor-oriented pharmacophore-based *in silico* screening of human catechol *O*-methyltransferase for the design of antiparkinsonian drug. *Bull. Korean Chem. Soc.* **28,** 379–385
53. Nicolotti, O., Altomare, C., Pellegrini-Calace, M., and Carotti, A. (2004) Neuronal nicotinic acetylcholine receptor agonists. Pharmacophores, evolutionary QSAR, and 3D-QSAR models. *Curr. Top. Med. Chem.* **4,** 335–360
54. Singh, N., Nolan, T. L., and McCurdy, C. R. (2008) Chemical function-based pharmacophore development for novel, selective kappa opioid receptor agonists. *J. Mol. Graph. Model.* **27,** 131–139
55. Clayton, T., Chen, J. L., Ernst, M., Richter, L., Cromer, B. A., Morton, C. J., Ng, H., Kaczorowski, C. C., Helmstetter, F. J., Furtmüller, R., Ecker, G., Parker, M. W., Sieghart, W., and Cook, J. M. (2007) An updated unified pharmacophore model of the benzodiazepine binding site on γ-aminobutyric acid(a) receptors. Correlation with comparative models. *Curr. Med. Chem.* **14,** 2755–2775
56. Li, Y., and Harte, W. E. (2002) A review of molecular modeling approaches to pharmacophore models and structure-activity relationships of ion channel modulators in CNS. *Curr. Pharm. Des.* **8,** 99–110
57. Fossa, P., Menozzi, G., and Mosti, L. (2001) An updated topographical model for phosphodiesterase 4 (PDE4) catalytic site. *Quant. Struct. Act. Relat.* **20,** 17–22
58. Fan, J. Q., and Ishii, S. (2003) Cell-based screening of active-site specific chaperone for the treatment of Fabry disease. *Methods Enzymol.* **363,** 412–420
59. Ishii, S., Yoshioka, H., Mannen, K., Kulkarni, A. B., and Fan, J. Q. (2004) Transgenic mouse expressing human mutant α-galactosidase A in an endogenous enzyme deficient background. A biochemical animal model for studying active-site specific chaperone therapy for Fabry disease. *Biochim. Biophys. Acta* **1690,** 250–257
60. Cohen, F. E., and Kelly, J. W. (2003) Therapeutic approaches to protein-misfolding diseases. *Nature* **426,** 905–909
61. Riordan, J. R. (2008) CFTR function and prospects for therapy. *Annu. Rev. Biochem.* **77,** 701–726
62. Van Goor, F., Straley, K. S., Cao, D., González, J., Hadida, S., Hazlewood, A., Joubran, J., Knapp, T., Makings, L. R., Miller, M., Neuberger, T., Olson, E., Panchenko, V., Rader, J., Singh, A., Stack, J. H., Tung, R., Grootenhuis, P. D., and Negulescu, P. (2006) Rescue of ΔF508-CFTR trafficking and gating in human cystic fibrosis airway primary cultures by small molecules. *Am. J. Physiol. Lung Cell. Mol. Physiol.* **290,** L1117–L1130
63. Kalid, O., Mense, M., Fischman, S., Shitrit, A., Bihler, H., Ben-Zeev, E., Schutz, N., Pedemonte, N., Thomas, P. J., Bridges, R. J., Wetmore, D. R., Marantz, Y., and Senderowitz, H. (2010) Small molecule correctors of F508del-CFTR discovered by structure-based virtual screening. *J. Comput. Aided Mol. Des.* **24,** 971–991
64. Pedemonte, N., Lukacs, G. L., Du, K., Caci, E., Zegarra-Moran, O., Galietta, L. J., and Verkman, A. S. (2005) Small-molecule correctors of defective ΔF508-CFTR cellular processing identified by high-throughput screening. *J. Clin. Invest.* **115,** 2564–2571
65. Pedemonte, N., Tomati, V., Sondo, E., and Galietta, L. J. (2010) Influence of cell background on pharmacological rescue of mutant CFTR. *Am. J. Physiol. Cell Physiol.* **298,** C866–C874
66. Brady, R. O., Gal, A. E., Bradley, R. M., Martensson, E., Warshaw, A. L., and Laster, L. (1967) Enzymatic defect in Fabry's disease. Ceramidetrihexosidase deficiency. *N. Engl. J. Med.* **276,** 1163–1167
67. Lemansky, P., Bishop, D. F., Desnick, R. J., Hasilik, A., and von Figura, K. (1987) Synthesis and processing of α-galactosidase A in human fibroblasts. Evidence for different mutations in Fabry disease. *J. Biol. Chem.* **262,** 2062–2065
68. Askari, H., Kaneski, C. R., Semino-Mora, C., Desai, P., Ang, A., Kleiner, D. E., Perlee, L. T., Quezado, M., Spollen, L. E., Wustman, B. A., and Schiffmann, R. (2007) Cellular and tissue localization of globotriaosylceramide in Fabry disease. *Virchows Arch.* **451,** 823–834
69. Zarate, Y. A., and Hopkin, R. J. (2008) Fabry's disease. *Lancet* **372,** 1427–1435
70. Yam, G. H., Zuber, C., and Roth, J. (2005) A synthetic chaperone corrects the trafficking defect and disease phenotype in a protein misfolding disorder. *FASEB J.* **19,** 12–18
71. Benjamin, E. R., Flanagan, J. J., Schilling, A., Chang, H. H., Agarwal, L., Katz, E., Wu, X., Pine, C., Wustman, B., Desnick, R. J., Lockhart, D. J., and Valenzano, K. J. (2009) The pharmacological chaperone 1-deoxygalactonojirimycin increases α-galactosidase A levels in Fabry patient cell lines. *J. Inherit. Metab. Dis.* **32,** 424–440
72. Khanna, R., Soska, R., Lun, Y., Feng, J., Frascella, M., Young, B., Brignol, N., Pellegrino, L., Sitaraman, S. A., Desnick, R. J., Benjamin, E. R., Lockhart, D. J., and Valenzano, K. J. (2010) The pharmacological chaperone 1-deoxygalactonojirimycin reduces tissue globotriaosylceramide levels in a mouse model of Fabry disease. *Mol. Ther.* **18,** 23–33
73. Hughes, D., Adera, M., Castelli, J., Bragat, A., Marsden, D. L., and Boudes, P. B. (2010) Preliminary long-term safety, tolerability, and assessments of renal function of adult Fabry patients receiving treatment with AT1001 (migalastat hydrochloride), a pharmacological chaperone, for up to 3 years. *J. Inherit. Metab. Dis.* **33,** Suppl. 1, S148 (abstr.)
74. (2009) Phase III trial evaluating Amigal for the treatment of Fabry disease. *Mol. Ther.* **17,** 1309
75. Vogelstein, B., Lane, D., and Levine, A. J. (2000) Surfing the p53 network. *Nature* **408,** 307–310
76. Brown, C. J., Lain, S., Verma, C. S., Fersht, A. R., and Lane, D. P. (2009) Awakening guardian angels. Drugging the p53 pathway. *Nat. Rev. Cancer* **9,** 862–873
77. Wiman, K. G. (2010) Pharmacological reactivation of mutant p53. From protein structure to the cancer patient. *Oncogene* **29,** 4245–4252
78. Foster, B. A., Coffey, H. A., Morin, M. J., and Rastinejad, F. (1999) Pharmacological rescue of mutant p53 conformation and function. *Science* **286,** 2507–2510
79. Bykov, V. J., Issaeva, N., Zache, N., Shilov, A., Hultcrantz, M., Bergman, J., Selivanova, G., and Wiman, K. G. (2005) Reactivation of mutant p53 and induction of apoptosis in human tumor cells by maleimide analogs. *J. Biol. Chem.* **280,** 30384–30391
80. Boeckler, F. M., Joerger, A. C., Jaggi, G., Rutherford, T. J., Veprintsev, D. B., and Fersht, A. R. (2008) Targeted rescue of a destabilized mutant of p53 by an *in silico* screened drug. *Proc. Natl. Acad. Sci. U.S.A.* **105,** 10360–10365
81. Bykov, V. J., Issaeva, N., Shilov, A., Hultcrantz, M., Pugacheva, E., Chumakov, P., Bergman, J., Wiman, K. G., and Selivanova, G. (2002) Restoration of the tumor suppressor function to mutant p53 by a low-molecular-weight compound. *Nat. Med.* **8,** 282–288
82. Wang, W., and El-Deiry, W. S. (2008) Restoration of p53 to limit tumor growth. *Curr. Opin. Oncol.* **20,** 90–96
83. Lambert, J. M., Moshfegh, A., Hainaut, P., Wiman, K. G., and Bykov, V. J. (2010) Mutant p53 reactivation by PRIMA-1^{MET} induces multiple signaling pathways converging on apoptosis. *Oncogene* **29,** 1329–1338
84. Lambert, J. M., Gorzov, P., Veprintsev, D. B., Söderqvist, M., Segerbäck, D., Bergman, J., Fersht, A. R., Hainaut, P., Wiman, K. G., and Bykov, V. J. (2009) PRIMA-1 reactivates mutant p53 by covalent binding to the core domain. *Cancer Cell* **15,** 376–388